Chapter 1

PHASE CONTROLLED FEMTOSECOND LASERS FOR SENSITIVE, PRECISE, AND WIDE BANDWIDTH NONLINEAR SPECTROSCOPY

Jun Ye
JILA, National Institute of Standards and Technology and University of Colorado, Boulder, Colorado 80309-0440, USA, email: Ye@jila.colorado.edu

Abstract: Recent progress in precision control of pulse repetition rate and carrier-envelope phase of ultrafast lasers has established a strong connection between optical frequency metrology and ultrafast science. A wide range of applications has ensued, including measurement of absolute optical frequencies, precision laser spectroscopy, optical atomic clocks, and optical frequency synthesis in the frequency-domain, along with pulse timing stabilization, coherent synthesis of optical pulses, and phase-sensitive extreme nonlinear optics in the time-domain. In this chapter we discuss the impact of the femtosecond optical frequency comb to atomic and molecular spectroscopy. Measurements performed in the frequency-domain provide a global picture of atomic and molecular structure at high precision while providing radio frequency clock signals derived from optical standards. Time-domain analysis and experiments give us new possibilities for nonlinear optical spectroscopy and sensitive detections with real-time information.

Key words: Phase control, femtosecond lasers, optical comb, precision frequency metrology, nonlinear spectroscopy.

1. INTRODUCTION TO FEMTOSECOND OPTICAL FREQUENCY COMB

Precise phase control of femtosecond lasers has become increasingly important as novel applications utilizing the femtosecond laser-based optical comb are developed that require greater levels of precision and higher

degrees of coherence and control.[1] Improved stability is beneficial for both frequency-domain applications, where the relative phase or "chirp" between comb components is unimportant (e.g. optical frequency metrology), and, perhaps more importantly, time-domain applications where the pulse shape and/or duration are vital, such as in nonlinear optical interactions.[2] For both types of applications, minimizing jitter in the pulse train and noise in the carrier-envelope phase is often critical to achieve the desired level of precision and coherence. Phase-stabilized mode-locked femtosecond lasers have played a key role in recent advances in optical frequency measurement,[3-5] carrier-envelope phase stabilization,[2, 6, 7] all-optical atomic clocks,[8, 9] optical frequency synthesizers,[10] coherent pulse synthesis,[11] and broadband, phase-coherent spectral generation.[12]

Mode-locked lasers generate short optical pulses by establishing a fixed phase relationship between all of the lasing longitudinal modes. To understand the connection between the time-domain and frequency-domain descriptions of a mode-locked laser and the pulse train that it emits, a key concept is the carrier-envelope phase. This is based on the decomposition of the pulses into an envelope function, $\hat{\mathrm{E}}(t)$, that is superimposed on a continuous carrier wave with frequency ω_c, so that the electric field of the pulse is written as $\mathrm{E}(t) = \hat{\mathrm{E}}(t)e^{i\omega_c t}$. The carrier-envelope phase, ϕ_{CE}, is the phase shift between the peak of the envelope and the closest peak of the carrier wave. In any dispersive material, the difference between group and phase velocities will cause ϕ_{CE} to evolve. This group-phase velocity mismatch inside a laser cavity produces a pulse-to-pulse phase shift accumulated over one round-trip as $\Delta\phi_{CE}$.

When ϕ_{CE} is constant, the spectrum of a femtosecond optical comb corresponds to identical pulses emitted by the mode-locked laser. For a single pulse, the spectrum is the Fourier transform of its envelope function and is centered at the optical frequency of its carrier. Generally, for any pulse shape, the frequency width of the spectrum will be inversely proportional to the temporal width of the envelope. For a train of identical pulses, separated by a fixed interval, the spectrum can easily be obtained by a Fourier series expansion, yielding a comb of regularly spaced frequencies, where the comb spacing is inversely proportional to time interval between successive pulses, i.e., the inverse of the repetition rate f_{rep} of the laser. The Fourier relationship between time and frequency resolution guarantees that any spectrometer with sufficient spectral resolution to distinguish the individual comb lines cannot have enough temporal resolution to separate successive pulses. Therefore the successive pulses interfere with each other inside the spectrometer and the comb spectrum occurs because there are certain discrete frequencies at which the interference is constructive. Using the result from Fourier analysis that a shift in time corresponds to a linear

phase change with frequency, we can readily see that the constructive interference occurs at $n f_{rep}$, where n is an integer.

When ϕ_{CE} is evolving with time, such that from pulse to pulse (with a time separation of $T = 1/f_{rep}$) there is a phase shift of $\Delta\phi_{CE}$, then in the spectral domain a rigid shift will occur for the frequencies at which the pulses add constructively. This shift is easily determined as $(1/2\pi)\,\Delta\phi_{CE}/T$. Thus the optical frequencies, ν_n, of the comb lines is written as $\nu_n = n f_{rep} + f_0$ where n is a large integer of order 10^6 that indexes the comb line, and f_0 is the comb offset due to pulse-to-pulse phase shift, $f_0 = (1/2\pi) f_{rep}\,\Delta\phi_{CE}$. The relationship between time- and frequency-domain pictures is summarized in Fig. 1-1. The pulse-to-pulse change in the phase for the train of pulses emitted by a mode-locked laser can be expressed in terms of the average phase (v_p) and group (v_g) velocities inside the cavity. Specifically, $\Delta\phi_{CE} = (1/v_g - 1/v_p)\, l_c \omega_c$, where l_c is the round-trip length of the laser cavity and ω_c is the "carrier" frequency.

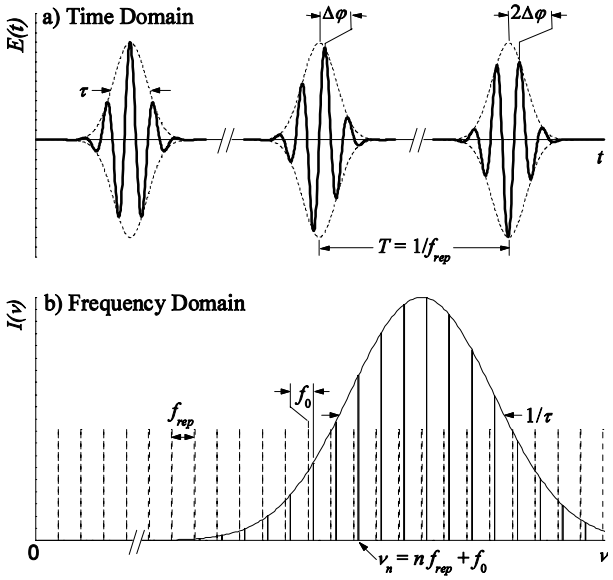

Figure 1-1. Summary of the time-frequency correspondence for a pulse train with evolving carrier-envelope phase.

Armed with the understanding of the frequency spectrum of a mode-locked laser, we now turn to the question of measuring the absolute frequencies of comb lines. For a frequency measurement to be absolute, it must be referenced to the hyperfine transition of ^{133}Cs that defines the second. From the relations listed above we see that determining the absolute optical frequencies of the femtosecond comb requires two radio frequency

(RF) measurements, that of f_{rep} and f_0. Measurement of f_{rep} is straightforward; we simply detect the pulse train's repetition rate (from tens of MHz to several GHz) with a fast photodiode. On the other hand, measurement of f_0 is more involved as the pulse-to-pulse carrier envelope phase shift requires interferometric measurement, whether it is carried out in the time-domain[13] or in the frequency-domain.[14] When the optical spectrum spans an octave in frequency, i.e., the highest frequencies are a factor of two larger than the lowest frequencies in the spectrum, measurement of f_0 is greatly simplified. If we use a second harmonic crystal to frequency double a comb line, with index n, from the low frequency portion of the spectrum, it will have approximately the same frequency as the comb line on the high frequency side of the spectrum with index $2n$. Measuring the heterodyne beat between these two families of optical comb lines yields a difference frequency by $2\nu_n - \nu_{2n} = 2(nf_{rep} + f_0) - (2nf_{rep} + f_0) = f_0$, which is just the offset frequency. Thus an octave-spanning spectrum enables a direct measurement of f_0 .[6] Note that an octave-spanning spectrum is not required, it just represents the simplest approach. We designate this scheme, shown in Fig. 1-2(a), as "self-referencing" since it uses only the output of the mode-locked laser. Self-referencing is not the only means of determining the absolute optical frequencies given an octave-spanning spectrum. For example, the absolute optical frequency of a CW laser can be determined if its frequency lies close to comb line n in the low frequency portion of the femtosecond comb spectrum. Then the second harmonic of the CW laser will be positioned close to the comb line $2n$. Measurement of the heterodyne beat between the CW laser frequency, ν_s , and the comb line n gives $f_{beat1} = \nu_s - (nf_{rep} + f_0)$ and between the second harmonic of the CW laser and comb line $2n$ gives $f_{beat2} = 2\nu_s - (2nf_{rep} + f_0)$. Mixing the beats with appropriate weighting factors gives $f_{beat2} - 2f_{beat1} = 2\nu_s - (2nf_{rep} + f_0) - (2\nu_s - 2(nf_{rep} + f_0)) = f_0$, which represents the second detection scheme shown in Fig. 1-2(b).[9]

An octave-bandwidth optical comb is not straightforward to produce. A Fourier-transform limited pulse with a full width at half maximum (FWHM) bandwidth of an octave centered at 800 nm would only be a single optical cycle in duration. Such short pulses have not been achieved. Fortunately, neither a transform-limited pulse nor a FWHM of an octave is actually needed. The pulse width is unimportant as the measurement and control techniques are purely frequency domain approaches. Experimentally, it has been found that even if the power at the octave spanning points is 40 dB below the peak, it is still possible to observe strong f-to-2f heterodyne beats. Still, the necessary comb bandwidth is larger than that from a typical sub-10-fs mode-locked Ti:sapphire laser. One approach to produce this sufficient spectral bandwidth is based on self-phase modulation directly inside the Ti:Sapphire crystal itself[15] or inside an additional glass plate located inside

the laser cavity with secondary coincident time and space foci.[16] These techniques require carefully designed mirrors and laser cavities. Additional spectral bandwidth can also be obtained by minor changes in the cavity configuration of a high repetition rate laser, although it has not yet yielded sufficient intensity at the octave points for the observation of f-to-2f beats.[17] Another widely adopted approach is to generate the extra comb bandwidth using microstructure fibers that have zero group velocity dispersion (GVD) within the emission spectrum of a Ti:sapphire laser.[18] The large index contrast for waveguiding inside microstructure fibers has two consequences; first the ability to generate a zero in the GVD at visible or near-infrared wavelengths and, secondly, the possibility of using a much smaller core size. This allows broadband continuum generation with only 10^{-9} J pulse energies.

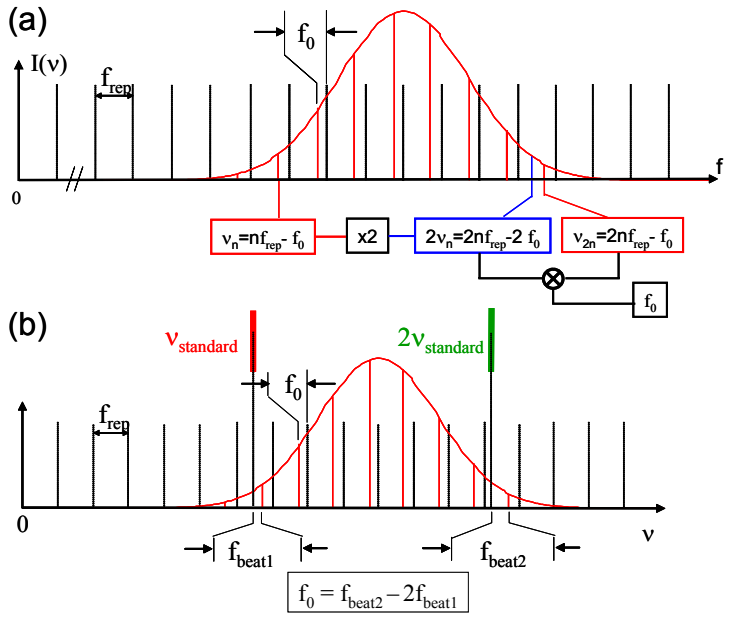

Figure 1-2. Two equivalent schemes for measurement of f_0 using an octave-spanning optical frequency comb. In the self-referencing approach, shown in (a), frequency doubling and comparison are accomplished with the comb itself. In the second approach shown in (b), the fundamental frequency ($\nu_{standard}$) and its second harmonic of a CW optical standard are used to determine f_0 . These two basic schemes are employed for absolute optical frequency measurement and implementation of optical atomic clocks.

For the purpose of using a femtosecond optical comb for absolute optical frequency measurements, it is straightforward to establish the frequency values of all of the comb components. The comb's frequency spacing (f_{rep}) can be phase locked with high precision via detection of higher harmonics of

f_{rep} relative to an RF standard. The value of f_0 is determined and controlled using schemes shown in Fig. 1-2. Control of f_0 requires a servo transducer acting differentially on the intracavity group and phase delays. One common method for adjusting f_0 is to swivel the end mirror in the arm of the laser cavity that contains the prism sequence.[19] An alternative method of controlling f_0 is via modulation of the pump power, with likely contributions from the nonlinear phase, spectral shifts, and the intensity dependence in the group velocity.[20] It is worth noting that a scheme implemented by Telle *et al*.[21] allows the frequency comb to be free running (without any active stabilization) while making highly precise measurement or connection for an optical frequency interval located within the comb bandwidth.

The dramatic simplification of a complex optical frequency chain to that of a single mode-locked laser has greatly facilitated optical frequency measurement. Another important aspect of this new technology is its high degree of reliability and precision and lack of systematic errors. For example, recent tests have shown that the repetition rate of a mode locked laser equals the mode spacing of the corresponding comb to within the measurement uncertainty of 10^{-16}. The uniformity of the comb mode spacing has also been verified to a level below 10^{-17}, even after spectral broadening in a fiber.[3,4] Comparison between two separate fs comb systems, both linked to a common reference source (microwave or optical), allows one to examine the intrinsic accuracy of a femtosecond-comb-based frequency measurement system, currently at a level of a few parts in 10^{16} with no measurable systematic effects.[22] Direct comparisons of absolute optical frequency measurements between the femtosecond comb technique and the traditional harmonic frequency chain approach have also produced assuring mutual confirmations at the 10^{-12} to 10^{-14} level.[5, 23]

As the measurement precision for optical frequencies continues to advance, the stability limitation imposed by available RF standards used for fs comb stabilization becomes an important issue.[23, 24] Instead of operating a fs comb using RF references, it appears to be advantageous to operate the comb by stabilizing it to an optical frequency standard. The fs comb in turn produces optically derived stable clock signals in the RF domain, leading to a so-called “optical atomic clock”.[8, 9, 25] Recent experimental demonstrations support the concept that, in the future, the most stable and accurate frequency standards will be based on optical transitions.[26, 27] Stepping down the stability level by one or two orders of magnitude, portable optical frequency standards that offer compact, simple, and less expensive system configurations have also shown competitive performance with (in-)stability near 10^{-14} at 1 to 10 s averaging time.[28]

To realize an optical atomic clock, an optical comb needs to be stabilized to a pre-selected optical frequency source at a precision level that exceeds

the optical standard itself. f_0 can be extracted in a straightforward manner using either schemes shown in Fig. 1-2. f_0 is then stabilized with respect to either f_{rep} or an auxiliary stable RF source. It is worth noting that stabilization of f_0 at a few mHz is more than adequate, as it yields fractional frequency noise of $< 10^{-17}$ for an optical carrier. A heterodyne beat between one of the comb components and the optical standard (ν_s) yields information about fluctuations in f_{rep} . For the particular case shown in Fig. 1-2(b), $f_{beat2} - f_{beat1} = 2\nu_s - (2nf_{rep} + f_0) - (\nu_s - (nf_{rep} + f_0)) = \nu_s - nf_{rep}$, producing a direct link between the frequencies ν_s and f_{rep} . After appropriate processing, this error signal is used to stabilize the phase of f_{rep} coherently to ν_s, thereby producing an output clock signal in the RF domain derived from ν_s.

Besides the capability of deriving RF signals from an optical frequency standard, a fs comb can, of course, also be used to transfer the stability of optical standards across vast frequency gaps to other optical spectral regions. Easy access to the resolution and stability offered by optical standards will greatly facilitate the application of frequency metrology to precise spectroscopic investigations. For spectroscopy applications, we indeed often desire a single-frequency and reasonably powered optical carrier wave that can be tuned to any desired optical spectral feature of interest. Realization of such an optical frequency synthesizer (analogous to its RF counterpart) will add a tremendously useful tool for modern spectroscopy experiments. Ideally one would realize a high precision optical frequency synthesizer based on a stable fs comb linked to an optical frequency standard. One could foresee an array of diode lasers, each covering a successive tuning range of ~ 10 to 20 nanometers that would collectively cover most of the visible spectrum. Each diode laser frequency would be controlled by the stabilized optical comb, and therefore be directly related to the absolute time/frequency standard in a phase coherent fashion, while the setting of the optical frequency would be accomplished via computer control.

In our preliminary implementation of such an optical frequency synthesizer,[10] the fs comb system is referenced by an I_2-based optical frequency standard at 532 nm. A CW diode laser, as well as a CW Ti:sapphire laser, is used to tune through targeted spectral regions (for example, Rb D1 and D2 lines at 795 and 780 nm for the diode laser and I_2 hyperfine transitions in the region of 490 - 520 nm) with desired frequency step sizes, while maintaining absolute reference to the stabilized optical comb. A self-adaptive search algorithm first tunes the CW laser to a specified wavelength region with the aid of a wavelength measurement device (100 MHz resolution). A heterodyne beat signal between the laser's frequency and that of a corresponding comb line is then detected and processed. For fine-tuning, an RF source provides a tunable frequency offset

for the optical beat. Once the laser frequency tuning exceeds f_{rep}, we reset the RF offset frequency back to the original value to start the process over again. The laser frequency can thus be tuned smoothly in an "inch-worm" manner along the comb structure. We have demonstrated two fundamental aspects of an optical frequency synthesizer; namely continuous, precise tuning of the optical frequency as well as arbitrary frequency setting on demand. The entire search process takes about a minute.

2. PRECISION ATOMIC SPECTROSCOPY – STRUCTURE AND DYNAMICS

The first example of spectroscopic application of a precisely stabilized femtosecond comb centers on investigation of a two-photon transition in laser cooled Rb atoms. Phase coherence among the successive pulses interacting with a cold atomic sample brings immediately to mind the approach of Ramsey interference for precision atomic spectroscopy. However, the difference here is that the bandwidth associated with the femtosecond pulse is so broad that one is enabled to explore the structure of a large number of atomic states all at once, along with the possibility of studying coherent accumulation in a multilevel system.[29] It is thus possible to simultaneously explore the global structure and dynamics of an atomic system. The multi-pulse interference in the time domain gives an interesting variation and generalization of the two-pulse based temporal coherent control of the excited state wavepacket.

From the frequency domain perspective, it is also straightforward to appreciate the fact that the spectroscopic resolution and precision will not be compromised by the use of ultrafast pulses since they are associated with a phase-stabilized, wide-bandwidth femtosecond comb. Phase coherence among various transition pathways through different intermediate states produces multi-path quantum interference effects on the resonantly enhanced two-photon transition probability in the cold Rb atoms. The two-photon transition spectrum can be analyzed in terms of the pulse repetition rate (f_{rep}) and the carrier-envelope offset frequency (f_0).[30] Both can be stabilized to high precision. With a set of measurements taken at a few different, but predetermined, combinations of f_{re} and f_0, one can essentially derive all relevant atomic energy level positions in absolute terms.

Doppler-free two-photon spectroscopy is carried out usually with two equal-frequency cw laser beams propagating in opposite directions. The two-photon transition rate can be resonantly enhanced via the intermediate states with two different laser frequencies[31] or accelerated atomic beams,[32] with a small residual Doppler effect. High-resolution two-photon spectroscopy

using pulsed light has also been demonstrated,[33] with the recent extension to cold atoms.[34] The unique feature of the present work is that the wide bandwidth optical comb allows all relevant intermediate states to resonantly participate in the two-photon excitation process, permitting the phase coherence among different comb components to induce a stronger transition rate through quantum interference. Following the initial proposal and the subsequent theoretical investigations, we are exploring experimentally this novel, high-resolution spectroscopy using a femtosecond laser.[35]

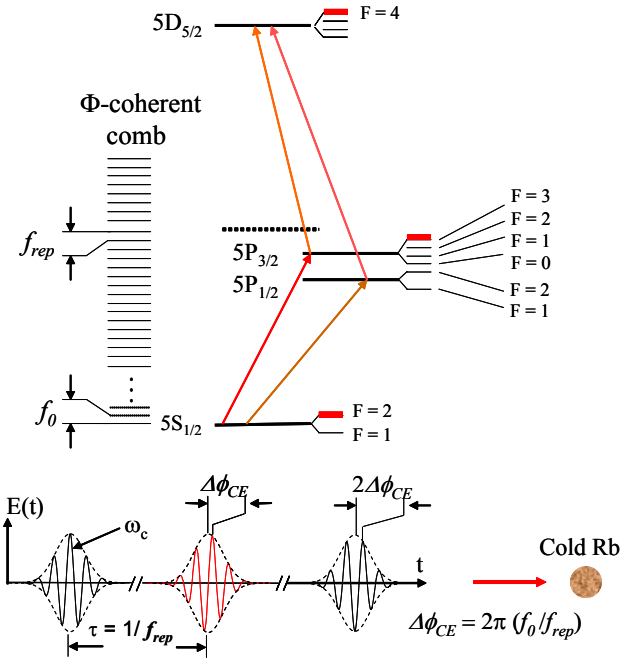

Figure 1-3. Top: Schematic of the relevant energy levels of the ^{87}Rb atom and the frequency-domain perspective of the atom-light interaction. Bottom: Time-domain picture showing a sequence of mode-locked pulses, with the relevant interaction parameters in f_{rep} and $\Delta\phi_{CE}$.

Figure 1-3 shows the relevant ^{87}Rb energy levels involved in the two-photon transition from the ground state $5S_{1/2}$ to the excited state $5D_{3/2}$. The dipole-allowed intermediate states, $5P_{3/2}$ and $5P_{1/2}$, are located ~ 2 nm and 17 nm below the virtual level, respectively. Also shown is a regularly spaced comb of optical frequencies around 800 nm. The experimental bandwidth of the comb is ~ 50 nm, emitted from a 10 fs, 100 MHz repetition-rate mode-locked Ti:sapphire laser. Adjustment of f_{rep} and f_0 allows the comb components to line up with corresponding hyperfine states of $5P_{3/2}$ and $5P_{1/2}$ to resonantly enhance the two-photon transition. This dependence of the

multi-path quantum interference on f_{rep} and f_0 leads to simultaneous stabilization of both quantities, and thereby the entire comb. The frequency-domain analysis is complemented by the time domain multi-pulse Ramsey interference picture, as illustrated in Fig. 1-3, where the relevant quantities for interaction are $\tau = 1/f_{rep}$ and $\Delta\phi_{CE}$. Both the frequency-domain and the time-domain analyses produce the same result on the two-photon transition spectra when one assumes a static distribution among the relevant atomic states. However, to follow the time evolution of the system, it is necessary to explore the interaction dynamics from one pulse to the next, taking into account both the atomic coherence and the optical coherence. The general Liouville equation for the density-matrix components of the atomic states, along with phenomenological decay terms, are used to derive a set of Bloch equations describing the evolution of all relevant levels associated with the ground, the excited, and the intermediate states.

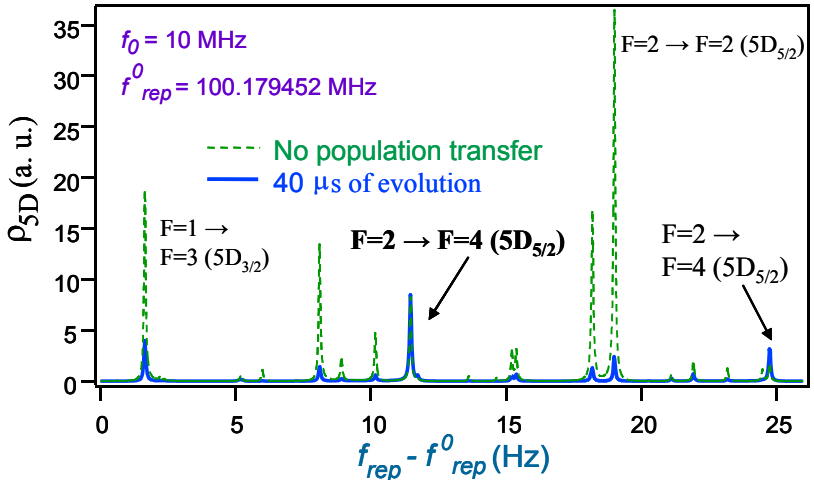

Figure 1-4. Density matrix calculation of the excited state population due to the two-photon transition induced by the phase-coherent fs pulse train. The nominal values of f_{rep} and f_0 are indicated. The spectrum given by the dashed line corresponds to the case with a static population while the spectrum given by solid line shows dynamic evolution after 4000 pulses.

Figure 1-4 illustrates the calculated population of the 5D states due to the two-photon transition, showing a clear evidence of population transfer when the number of interacting pulses increases. Not surprisingly, the most dominant transition pathway when a large number of pulses is involved is $5S_{1/2}$ (F=2) → $5P_{3/2}$ (F=3) → $5D_{5/2}$ (F=4), which represents a so-called closed transition. The horizontal axis represents a scanning of f_{rep} from its nominal value indicated in the figure. The actual optical frequency for the two-photon transition is near 385 THz, which represents a harmonic order of

3.85×10^6 of f_{rep} . Therefore, a change in f_{rep} by ~ 26 Hz implies a repeat in the optical comb spectrum near the two-photon transition region, and hence a repeat in the two-photon spectra.

Figure 1-5 shows experimental two-photon spectra resonantly enhanced by the intermediate states. We clearly confirm the predicted effect of population transfer by the pulse sequence when we compare the two spectra obtained under the influence of 1,200 and 250,000 pulses, respectively. Basically, the only transition pathway survived at the limit of a large number of pulses is $5S_{1/2}$ (F=2) → $5P_{3/2}$ (F=3) → $5D_{5/2}$ (F=4). It is interesting to note that we have also observed the pure two-photon transition pathway (energies of the two photons are degenerate) that is not resonantly enhanced by the intermediate states. The signal is indicated in Fig. 1-5 by a small peak (around 19 Hz) in the 2.5 ms evolution curve represented by diamonds, which repeats every 13 Hz in the scan of the f_{rep} value. This observation is consistent with the fact that a pure two-photon transition would repeat its signal every time the pulse spectrum is shifted by half of the repetition frequency. More recent work has pushed the spectroscopy resolution to the limit of the natural linewidth of 660 kHz associated with the D-state lifetime, owing to the use of ultracold atoms and careful control of photon momentum transfer. The work on this simple two-photon transition dynamics thus provides a solid link between the time-domain picture of carrier-envelope phase and the frequency-domain picture of f_{rep} and f_0. One practical consequence of these results is that we can now control both degrees of freedom for the femtosecond comb directly by a transition in cold atoms.

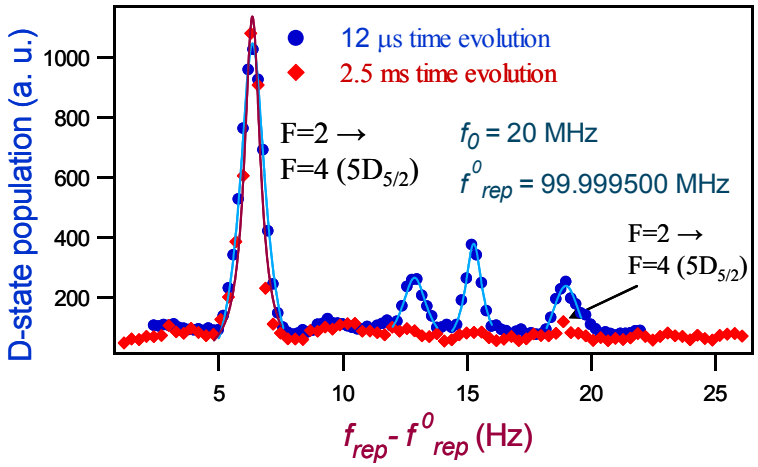

Figure 1-5. Experimental observation of resonantly enhanced two-photon transition with a clear influence by the pulse sequence on the atomic state dynamics.

3. MOLECULAR SPECTROSCOPY AIDED BY FEMTOSECOND OPTICAL FREQUENCY COMB

Before we study examples of molecular spectroscopy aided by the technology of the precision frequency comb, we would like to discuss briefly the implications of the frequency-domain control of the femtosecond laser to the time-domain experiments. Prior to the development of femtosecond comb technology, mode-locked lasers were used almost exclusively for time-domain experiments. Although the femtosecond comb technology has primarily impacted on the frequency-domain applications described earlier, it is having an impact on time-domain experiments and promises to bring about just as dramatic advances in the time-domain as it has in optical frequency metrology and optical clocks. Indeed, it is fascinating to blur the boundary between traditional CW precision spectroscopy and ultrafast phenomena. The time-domain applications put stringent requirements on the carrier-envelope phase coherence. Stabilization of the "absolute" carrier-envelope phase at a level of tens of milli-radians has been demonstrated and this phase coherence is maintained over an experimental period exceeding many minutes,[36] paving the groundwork for synthesizing electric fields with known amplitude and phase at optical frequencies. Working with two independent femtosecond lasers operating at different wavelength regions, we have synchronized the relative timing between the two pulse trains at the femtosecond level,[37] and also phase locked the two carrier frequencies, thus establishing phase coherence between the two lasers. By coherently stitching optical bandwidths together, a "synthesized" pulse has been generated.[11] With the same pair of Ti:sapphire mode-locked lasers, we have demonstrated widely tunable femtosecond pulse generation in the mid- and far-IR using difference-frequency-generation.[38] The flexibility of this new experimental approach is evidenced by the capability of rapid and programmable switching and modulation of the wavelength and amplitude of the generated IR pulses. A fully developed capability of producing phase-coherent visible and IR pulses over a broad spectral bandwidth, coupled with arbitrary control in amplitude and pulse shape, represents the ultimate instrumentation for coherent control of molecular systems. A pulse train with good carrier-envelope phase coherence is also very promising for experiments that are sensitive to ϕ_{CE}, i.e., the "absolute" pulse phase.[2] This can be manifested in "extreme" nonlinear optics experiments, or coherent control.

The capability to precisely control pulse timing and the pulse-carrier phase allows one to manipulate pulses using novel techniques and achieve unprecedented levels of flexibility and precision, as will be demonstrated in the work on time resolved spectroscopy of molecules. For example, the simultaneous control of timing jitter and carrier-envelope phase can be used

to phase coherently superpose a collection of successive pulses from a mode-locked laser. By stabilizing the two degrees of freedom of a pulse train to an optical cavity acting as a coherent delay, constructive interference of sequential pulses will be built up until a cavity dump is enabled to switch out the "amplified" pulse.[39] Such a passive pulse "amplifier", along with the synchronization technique we developed for pulse synthesis, has made a strong impact on the field of nonlinear-optics based spectroscopy and imaging of bio-molecular systems, showing significant improvements in experimental sensitivity and spatial resolution.[40, 41] With the enhanced detection sensitivity comes the capability of tracking real time biological dynamics. An ultrafast laser locked to a high stability cavity is also expected to demonstrate extremely low pulse jitter and carrier-envelope phase noise, which will be particularly attractive for time-domain experiments. In addition, we are exploring the use of pulse-cavity interactions to obtain a high sensitivity in intracavity spectroscopy (linear and non-linear) with a wide spectral coverage, as well as to enhance nonlinear interaction strengths for high efficiency nonlinear optical experiments.

With these new sets of tools in hand, it is appropriate to revisit the topics of precision molecular spectroscopy. It is also interesting to explore spectroscopy in a more broad sense. For example, one can now carry out precision spectroscopy using ultrafast lasers. On the other hand, coherent control of molecular motion can be performed in the spirit of precision measurement. The capability of absolute optical frequency measurements in the visible and IR spectral regions adds a new meaning to the term of precision molecular spectroscopy. Understanding of molecular structure and dynamics often involves detailed spectral analysis over a broad wavelength range. Such a task can now be accomplished with a desired level of accuracy uniformly across all relevant spectral windows, allowing precise investigations of minute changes in the molecular structure over a large dynamic range. For example, absolute frequency measurement of vibration overtone transitions and other related resonances (such as hyperfine splitting) reveals precise information about the molecular potential energy surface and relevant perturbation effects. We have pursued such a study in iodine molecules, performing high-resolution and high-precision measurement of hyperfine interactions of the first excited electronic state (B) of I_2 over an extensive range of vibrational and rotational quantum numbers towards the dissociation limit.[42] Experimental data demonstrate systematic variations in the hyperfine parameters that confirm calculations based on *ab initio* molecular potential energy curves and electronic wave functions derived from a separated-atomic basis set. We have accurately determined the state-dependent quantitative changes of hyperfine interactions caused by

perturbations from other electronic states and identified the respective perturbing states. Our work in I_2 near the dissociation limit is also motivated by the desire to improve cell-based portable optical frequency standards.[43] Indeed, I_2-stabilized lasers have already demonstrated high stability ($< 5 \times 10^{-14}$ at 1 s averaging time) and have served well for optical atomic clocks.[9]

4. I_2 HYPERFINE INTERACTIONS, OPTICAL FREQUENCY STANDARDS AND CLOCKS

The hyperfine structure of I_2 rovibrational levels includes four contributions: nuclear electric quadrupole (eqQ), spin-rotation (C), tensorial spin-spin (d), and scalar spin-spin (δ) interactions. Agreement between experiment and theory using the four-term effective hyperfine Hamiltonian is at the kilohertz level for a few selected transitions. For the first excited electronic state B with the $^2P_{3/2} + {}^2P_{1/2}$ dissociation limit, our goal is to perform a systematic high-precision investigation of hyperfine interactions over an extensive range of rovibrational quantum numbers coupled with a large range of internuclear separations. Such a study has allowed us to understand the rovibrational dependence of the hyperfine interactions (as well as the dependence on internuclear distance) based on *ab initio* molecular potential energy curves and the associated electronic wave functions. Careful analysis of various perturbation effects leads to precise determination of molecular structure over a large dynamic range.

Prior studies have concentrated on a few isolated rovibrational levels for the high vibrational levels $v' = 40$ to 82 in the B state.[44-46] For vibrational levels below $v' = 43$, only functional forms on the state-dependent variations of the hyperfine interactions have been investigated from empirical data.[47] Combining absolute optical frequency metrology with high-resolution and broad wavelength-coverage laser spectroscopy, we have measured ~ 80 rovibrational transitions with the upper vibrational levels (from $v' = 42$ up to $v' = 70$) stretching from a closely bonded molecular basis to a separated-atomic basis appropriate for the $^2P_{3/2} + {}^2P_{1/2}$ dissociation limit, providing kHz-level line accuracies for most hyperfine components. The study is performed in the wavelength region of 530 to 498 nm. Measurements performed on a large set of rovibrational quantum numbers provide systematic information on state-dependent variations in the hyperfine interactions caused by perturbation from other nearby states. Figure 1-6 shows a simple schematic of the ground and the first excited electronic states of I_2 and their relevant dissociation limits. The lower panel in Fig. 1-6 shows a clear trend of linewidth narrowing with decreasing transition wavelength. However, this tendency is complicated by variations in linewidths among

different rotational or hyperfine components when the transitions approach the pre-dissociation region. The initial linewidth narrowing at shorter wavelength may indicate among other interesting effects that the Franck-Condon factor in the transition probability is reduced when the excited state reaches a higher vibration level. As the excited state approaches the dissociation threshold, the limit on lifetime imposed by predissociation and other effects will need to be taken into consideration.

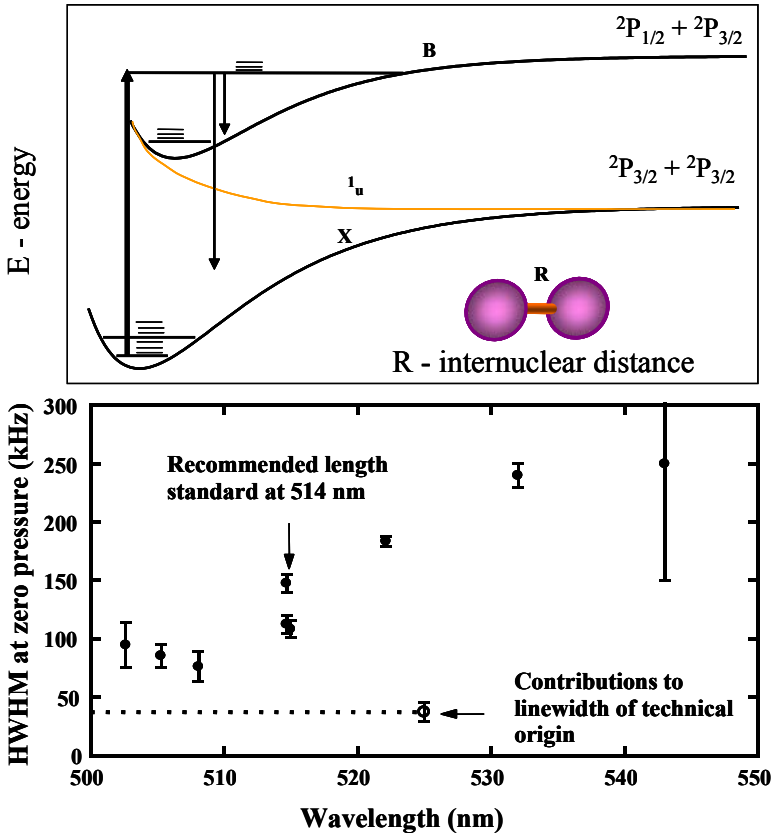

Figure 1-6. The ground state and the first excited state of I_2 with their associated dissociation limit. The lower panel shows a narrowing trend of the transition linewidth when the excited state approaches the dissociation limit.

Figure 1-7 illustrates the systematic rovibrational dependences for all four hyperfine parameters. Each solid line is a fit of the experimental data for rotational dependence belonging to a single vibrational level (v'). In general, all hyperfine parameters have a monotonic dependence on both rotational and vibrational quantum numbers except for the levels in the

vicinity of $v' = 57$ to 59. However, the v-dependence of eqQ_B reverses its trend after $v' = 60$. For the sake of figure clarity, the eqQ_B data for $v' > 60$ are not shown. Another important observation is that for levels of $v' = 57$ - 59 all hyperfine parameters except for C_B bear abnormal J-dependences due to perturbations from a 1_g state through accidental rotational resonances.

Combining data from this work and the literature,[47] investigations of the hyperfine spectra now cover the majority of the vibrational levels ($3 \le v' \le 82$) in the B state. Therefore, it is now possible and useful to explore the global trend of these hyperfine parameters in the B state. Suppressing the rotational dependence, hyperfine parameters as functions of pure vibrational energy $E(v')$ are found to increase rapidly when molecules approach the dissociation limit, which is a result of the increasingly strong perturbations from other high-lying electronic states sharing the same dissociation limit with the B state. While the variation of C_B is smooth over the whole range, eqQ_B, d_B, and δ_B all have local irregularities at three positions: $v' = 5$ where the B'':1_u state crosses nearby, around $v' = 57$ to 59 (see discussions above), and from $v' = 76$ to 78, due to the same 1_g state.[44, 46]

To examine these hyperfine parameters in terms of internuclear separation R, the vibrational average of the hyperfine parameters is removed by inverting the expression $O(v',J') = \langle v'_{J'} | O(R) | v'_{J'} \rangle$, where $O(v',J')$ denotes one of the four hyperfine parameters. Figure 1-7 plots eqQ_B, C_B, d_B, and δ_B against R-centroid evaluated from $\langle v'_{J'} | R | v'_{J'} \rangle$ (with $|v'_{J'}\rangle$ properly normalized), along with the corresponding residual errors of the interpolation. In Fig. 1-8(a), (b), (c), and (d), the solid lines are calculated from $\langle v'_{J'} | O(R) | v'_{J'} \rangle$ and the symbols are the experimental data. Consistent with C_B's smooth variation, the interpolation function C_B (R) has small residual errors (within ±0.03, relative) for the entire range from $v' = 3$ to 70. On the contrary, the large residual errors in the interpolation of eqQ_B, d_B, and δ_B for $v' \ge 56$ reflect their abnormal variations observed around $v' = 57$ and 59, restricting a reliable interpolation only to levels of $v' < 56$. In the region of $R < 5$ Å, valuable information can be readily extracted from eqQ_B to assist the investigation of I_2's electronic structure. Unlike the other three hyperfine parameters whose major parts originate from perturbations at nearly all possible values of R, a significant part of eqQ_B is due to the interaction between the nuclear quadrupole moment Q and the local electric field gradient $q(R)$ generated by the surrounding charge distribution of a largely B state character. Thus, for $R < 5$ Å, where perturbations from other electronic states are negligible, the vibration-removed interpolation function eqQ_B (R), coupled with *a priori* information on $q(R)$, can be used to determine I_2 nuclear quadrupole moment or serve as a benchmark for molecular *ab initio* calculations of the electronic structure at various values of R.

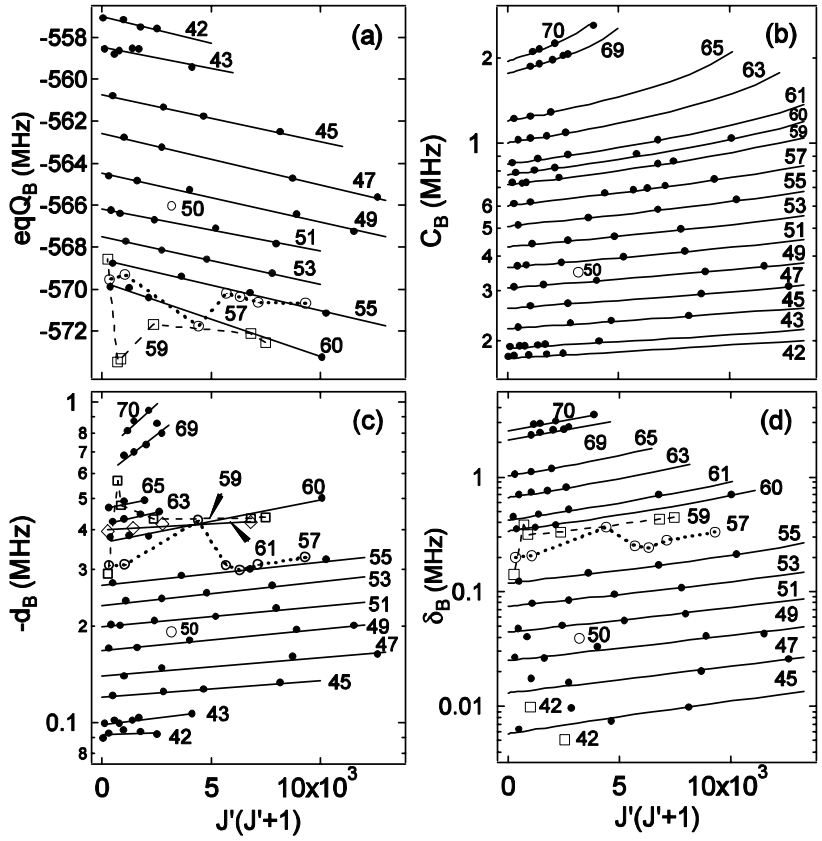

Figure 1-7. Rovibrational dependence of the *B* state hyperfine parameters (a) eqQ_B, (b) C_B, (c) d_B, and (d) δ_B. Note (b), (c), and (d) are semilog plots and the vertical scale of (c) has been inverted. Each solid line is a fit for *J*-dependence for each vibrational level (v' indicated in the figure). Experimental data in squares and open circles show abnormal variations of eqQ_B, d_B, and δ_B around $v' = 57$ and 59.

Precision measurements on *B*-*X* hyperfine spectra provide an alternative and yet effective way to investigate the potential energy curves (*PEC*s) sharing the same dissociation limit with the *B* state as well as the associated electronic wave functions. To demonstrate this, we perform calculations of eqQ_B, C_B, d_B, and δ_B based on the available *PEC*s and electronic wave functions derived from a separated-atomic basis set. For both vibrational and rotational dependences, the *ab initio* calculation results agree very well with the experimental data for $v' \geq 42$ (*R*-centroid $\geq$ 3.9 Å). In short, we have extended the range of separated-atomic basis calculations from levels near the dissociation limit to low vibrational levels ($v' = 5$) and have found very

good agreement with the experimental data on both vibrational and rotational dependences.

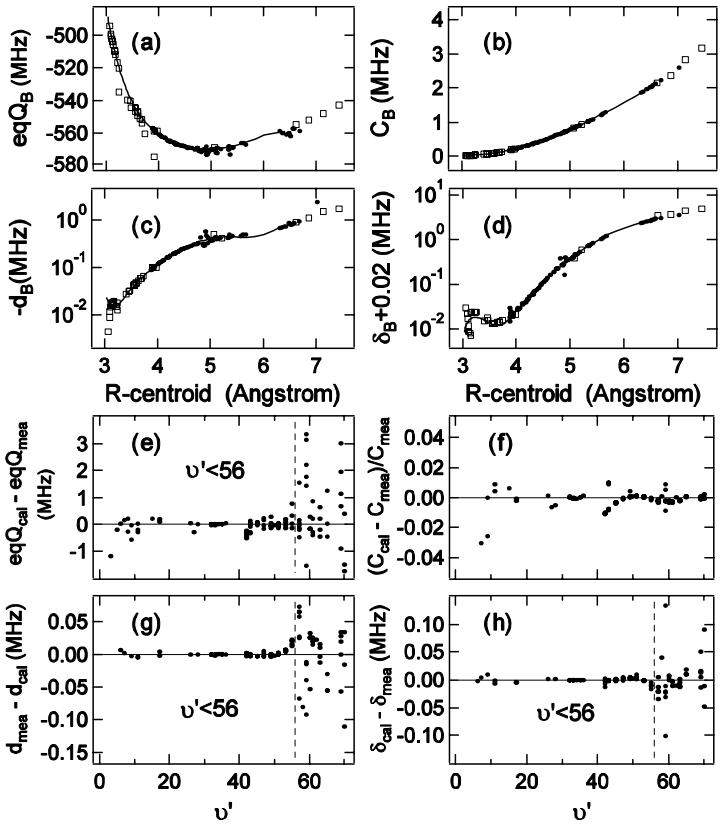

Figure 1-8. (a) eqQ_B, (b) C_B, (c) d_B, and (d) δ_B versus *R*-centroid. Solid lines are calculated from $\left\langle v'_{J'} \middle| O(R) \middle| v'_{J'} \right\rangle$. Symbols are experimental data (dots: this work, squares: literature). (e) - (h) show residual errors of the interpolation.

Besides these interesting studies in hyperfine structure, the narrow-linewidth I_2 transitions in this wavelength range also provide excellent cell-based optical frequency references for laser stabilization. Frequency-doubled Nd:YAG/$^{127}I_2$ at 532 nm has proved to be one of the best portable optical frequency standards with compact size, reliability, and high stability (< 5 x 10^{-14} at 1 s). To reach a better frequency stability, it is useful to explore I_2 transitions at wavelengths below 532 nm, where the natural linewidths decrease at a faster rate than the line strengths. We have measured the systematic variation of the I_2 transition linewidths within the range of 532 - 498 nm, with the linewidth decreasing by nearly 6 times when the wavelength is changed from 532 nm to near the dissociation limit.[43] The high *S/N* results indicate that I_2 transitions in the wavelength range 532 -

501 nm hold great promise for future development of optical frequency standards, especially with the advent of all solid state Yb:YAG lasers. One exciting candidate is the 514.67 nm standard,[48] with a projected stability < 10^{-14} at 1 s.

5. EXTEND PHASE-COHERENT FS COMBS TO THE MID-IR SPECTRAL REGION

Being able to combine the characteristics of two or more pulsed lasers working at different wavelengths certainly provides a more flexible approach to coherent control. The capability of synchronizing the repetition rates and phase-locking the carrier frequencies of two mode-locked lasers opens many applications. It may be particularly important in the generation of tunable femtosecond sources in other previously unreachable spectral regions. Figure 1-9 shows the cross-correlation measurement of the two stabilized mode-locked Ti:sapphire lasers using both sum (SFG) and difference frequency generation (DFG). The DFG signal produced by a GaSe crystal can be tuned from 6 micron and onto any longer wavelength regions with a high repetition rate (the same as the original laser's) and a reasonable average power (tens of microwatts). Arbitrary amplitude waveform generation and rapid wavelength switching in these nonlinear signals are simple to implement. The ultimate goal of this work is to make an optical waveform synthesizer that can create an arbitrary optical pulse on demand and use the novel source to study and control molecular motion. For frequency metrology and precision molecular spectroscopy in the IR region, we note that the difference frequency generation approach produces an absolute-frequency calibrated IR comb when the two Ti:sapphire lasers are synchronized and share a common offset frequency f_0.

One of the important spectral regions is 1.5 μm, where compact, reliable, and efficient mode-locked lasers exist and there is rich information on molecular spectroscopy. Frequency reference grids in this spectral window could also find applications in dense wavelength division multiplexed (DWDM) systems, photonic samplers in high-speed A/D conversion, and distribution of optical frequency standards over optical fiber networks. The synchronization and phase-locking approach for Ti:sapphire lasers can be extended to cover mode-locked lasers at 1.5 μm. We have indeed achieved tight synchronization and coherent phase locking between the repetition rates and the optical carriers, respectively, for the 1.5 μm mode-locked laser sources and a Ti:sapphire-based fs frequency comb, which is used as the clockwork for an optical atomic clock.

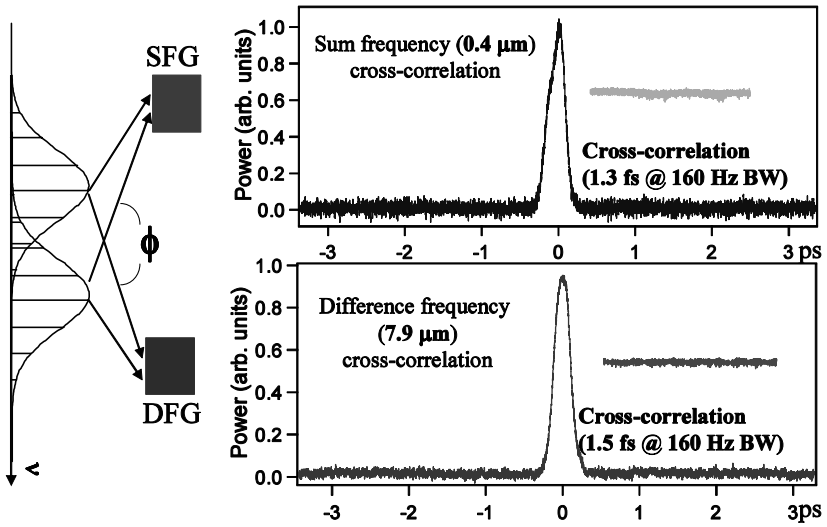

Figure 1-9. Simultaneous sum and difference frequency generations from two stabilized femtosecond lasers. Also shown are the amplitude fluctuations at the half power point due to the relative timing jitter between the two parent lasers.

A phase-coherent link between mode-locked lasers requires two distinct conditions to be met, as shown in Fig. 1-10(a). The comb spacing of the 1.5 μm source ($f_{rep,1550}$) must be stabilized to the optical clock's fs comb spacing ($f_{rep,775}$). Second, the combs' offset frequencies ($f_{0,775}$ and $f_{0,1550}$) must be phase locked together. This latter step requires spectral overlap between the two combs. The wide bandwidth optical frequency comb generated by the mode-locked fs Ti:sapphire laser is phase locked to a highly stable, iodine-based optical frequency standard. The optical comb of the 1.5 μm source is frequency doubled and compared against the Ti:sapphire comb at a mutually accessible spectral region to generate a heterodyne beat between the two combs.

Under simultaneous control of synchronization and phase locking, Fig. 1-10(b) shows frequency-counting records of the heterodyne beat signal between the 1.5 μm laser and the Ti:sapphire laser. At 1-s gate time, the rms fluctuation (σ_{rms}) of the heterodyne beat ($2 \times f_{0,1550} - f_{0,775}$) is reduced to 3.2 mHz, in sharp contrast to the 1.5 MHz rms fluctuation when $f_{0,1550}$ is not stabilized. By monitoring the beat error signal produced by the digital phase detector we ensure that no cycles have slipped for the phase locked loop over this measurement period. Allan deviation of the stabilized beat frequency record is shown in Fig. 1-10(c), determined with respect to the 1.5 μm optical carrier frequency.[49]

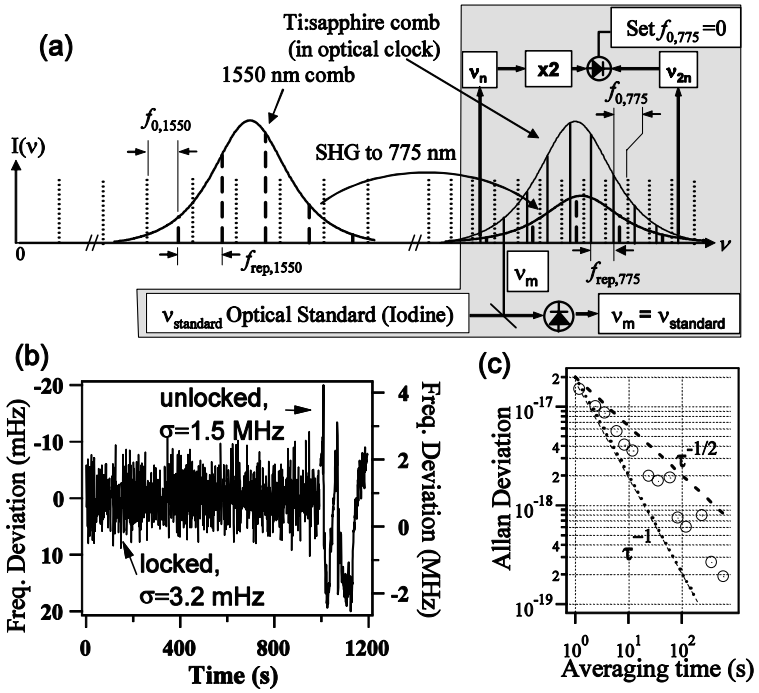

Figure 1-10. (a) Schematic diagram of simultaneous synchronization and phase locking between a 1.5 μm mode-locked laser diode and a 775-nm mode-locked Ti:sapphire laser. The shaded area shows the implementation of an optical clock based on a Ti:sapphire fs comb phase-stabilized to an iodine standard. The laser diode's repetition frequency is 8 times that of the Ti:sapphire (not as shown in the figure). (b) The heterodyne beat recorded by a frequency counter at 1 s gate time, under no phase locking (short trace, with respect to the right vertical axis) and phase locking (long trace, with respect to the left vertical axis). (c) The Allan deviation associated with the phase-locked signal.

6. FEMTOSECOND LASERS AND EXTERNAL OPTICAL CAVITIES

The combination of ultra-short pulses and optical cavities will open doors for a variety of exciting experiments. This requires the understanding of the intricate pulse-cavity interactions and the subsequent development of techniques to efficiently couple the ultra-short pulses into a high finesse optical cavity and coherently store them in the cavity. An immediate impact is on precision stabilization of ultrafast lasers.[50] Similar to the state-of-art stabilization of CW lasers, a cavity-stabilized ultrafast laser is expected to

demonstrate superior short-term stability of both the pulse repetition frequency and the carrier-envelope phase. The improved stability is beneficial in particular for time-domain applications where the signal processing bandwidth is necessarily large. Another attractive application lies in broadband and ultrasensitive spectroscopy. The use of high finesse cavities has played a decisive role for enhancing sensitivity and precision in atomic and molecular spectroscopy. We expect a dramatic advancement in the efficiency of intracavity spectroscopy by exploiting the application of ultra-short pulses. In other words, a high detection sensitivity is achievable uniformly across the broad spectrum of the pulse. Applying cavity-stabilization techniques to femtosecond lasers, the comb structure of the probe laser can be precisely matched to the resonance modes of an empty cavity, allowing an efficient energy coupling for a spectroscopic probe. Molecular samples located inside the high finesse cavity will have a strong impact on the dispersive properties of the cavity. In fact it is this dispersion-related cavity-pulling effect that will aid our sensitive detection process when we analyze the light transmitted through the cavity. Preliminary data on spectrally resolved, time-domain ring down measurement for intracavity loss over the entire femtosecond laser bandwidth are already quite promising.

To develop sources for ultrafast nonlinear spectroscopy, a properly designed, dispersion-compensated cavity housing a nonlinear crystal will provide efficient nonlinear optical frequency conversion of ultrashort optical pulses at spectral regions where no active gain medium exists. Furthermore, by simultaneously locking two independent mode-locked lasers to the same optical cavity, efficient sum and/or difference frequency generation can be produced over a large range of wavelengths. Under a similar motivation, a passive cavity can be used to explore coherent superposition of ultra short pulses, with cavity stabilization providing the means to phase coherently superpose a collection of successive pulses from a mode-locked laser. The coherently enhanced pulse stored in the cavity can be switched out using a cavity-dumping element (such as a Bragg cell), resulting in a single phase-coherent amplified pulse. The use of a passive cavity also offers the unique ability to effectively amplify pulses at spectral regions where no suitable gain medium exists, such as for the infrared pulses from difference-frequency mixing or the UV light from harmonic generation. Unlike actively dumped laser systems, the pulse energy is not limited by the saturation of a gain medium or a saturable absorber needed for mode-locking. Instead, the linear response of the passive cavity allows the pulse energy to build up inside the cavity until limited by cavity loss and/or dispersive pulse spreading. Therefore storage and amplification of ultra-short pulses in the femtosecond regime requires precise control of the reflected

spectral phase of the resonator mirrors as well as the optical loss of the resonator. While the reflected group delay of the mirrors only changes the effective length of the resonator, the group delay dispersion (GDD) and higher-order derivatives of the group delay with respect to frequency affect the pulse shape. The net cavity GDD over the bandwidth of the pulse needs to be minimized in order to maintain the shape of the resonant pulse and allow for the coherent addition of energy from subsequent pulses. Figure 1-11 illustrates the evolution of a 50 fs pulse inside a cavity with a finesse of 3,140 under the conditions of zero cavity dispersion (dashed curve) and finite dispersion (solid curve). Three representative pulses at different stages of amplification are also shown to illustrate the pulse buildup process. Although the 50 fs pulse is stretched by the dispersive cavity, it is not severely distorted due to its coupling with the incident pulse train. If the incident pulses become too short, the cavity finesse too high, or the laser repetition frequency deviates significantly from the cavity free-spectral-range (FSR) frequency, the intra-cavity pulse may quickly pull apart into several pulses, and the meaning of a single pulse width would be lost.

We have applied the coherent pulse-stacking technique to both picosecond and femtosecond pulses. Initial studies have already demonstrated amplification of picosecond pulses of greater than 30 times at repetition rates of 253 kHz, yielding pulse energies greater than 150 nJ.[41] With significant room left for optimization of the cavity finesse (current value of ~ 350, limited by the cavity input-coupling mirror), we expect that amplifications greater than a hundred times are feasible, bringing pulse energies into the μJ range. While the use of picosecond pulses allows us to separate out complications arising from intra-cavity dispersion, for sub-100 femtosecond pulses, dispersive phase shifts in the cavity mirrors become an important topic. Preliminary results in enhancing low individual pulse energies for sub-50 fs pulses illustrate the importance of GDD control. The external enhancement cavity incorporated specially designed negative GDD low-loss mirrors to simultaneously compensate for the Bragg cell's 3 mm of fused silica and provide a high finesse. The input-coupling mirror transmission was ~ 0.8%, with a measured cavity finesse of 440. An intracavity energy buildup of ~ 130 is expected, leading to single pulse amplifications of approximately 52 for the current setup given the 40% dumping efficiency of our Bragg cell. The negative GDD mirrors were designed to only partially compensate for the total cavity dispersion. The remaining cavity GDD was estimated at +20 to +30 fs^2. Controlling the intracavity pressure allows fine-tuning of the net cavity GDD to zero. Experimental results are in good agreement with independent numerical calculations. The input pulses of 47-fs duration are experimentally enhanced

by a factor of ~ 120 inside the passive cavity, with the output pulses broadened only to ~ 49 fs.

An important application of these advanced pulse control technologies is in the field of nonlinear-optics based spectroscopy and nanoscale imaging. For example, using two tightly synchronized picosecond lasers, we are able to achieve significant improvements in experimental sensitivity and spatial resolutions for coherent anti-Stokes Raman scattering (CARS) microscopy.[40] Vibrational imaging based on CARS spectroscopy is a powerful method for acquisition of chemically selective maps of biological samples.[51, 52] In CARS microscopy, pulsed pump and Stokes beams are focused tightly to a single focal spot in the sample to achieve a high spatial resolution. The third order nonlinear interaction produces a signal photon that is blue-shifted (anti-Stokes signal) with respect to the incident beams. Strong CARS signals are obtained whenever the frequency difference between the pump and Stokes coincides with a Raman-active vibrational mode, which gives rise to the molecule-specific vibrational contrast in the image. Recent studies and technological improvements have demonstrated the exciting capability of CARS microscopy to attain high-resolution vibrational images of unstained living cells.

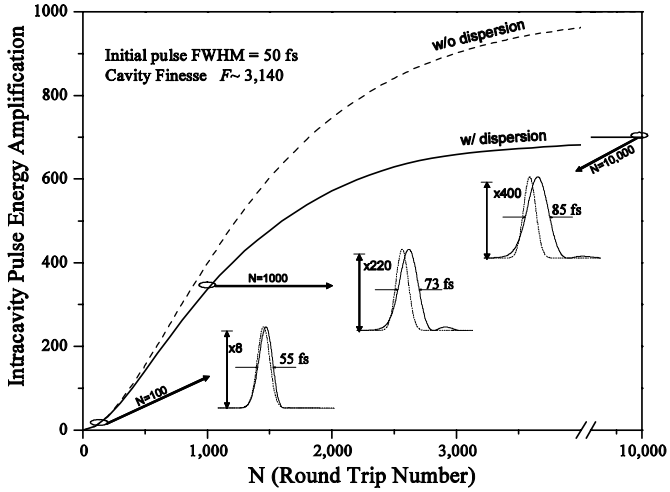

Figure 1-11. Coherent evolution of a 50 fs pulse inside the cavity. Dashed line indicates the ideal case of a dispersion-free cavity perfectly matched with the incident pulse train, while the solid line shows the effect of cavity dispersion in limiting the amount of energy coupled into the cavity.

Practical applications of the CARS microscopy technique require pulsed light sources: optimized peak powers help boost the nonlinear signal. Pulses with temporal widths of 1-2 picoseconds (ps) should be used to match to the vibration bandwidths in order to optimize the CARS signal, with minimized

non-resonant background and compromising spectral resolution. An important technical challenge is to achieve tight synchronization between two mode-locked lasers that produce the frequency difference that matches the vibrational resonance. Another important consideration is that while the repetition rate of the pulse train needs to be low enough to avoid thermal damage to the cell due to a high average power, the peak power of the pulses needs to be reasonably high to aid the nonlinear signal strength. A schematic setup combining CARS spectroscopy and pulse manipulation is shown in Fig. 1-12. The technologies of pulse synchronization and coherent pulse stacking therefore become ideal tools for carrying out this task of spectroscopy plus microscopy.

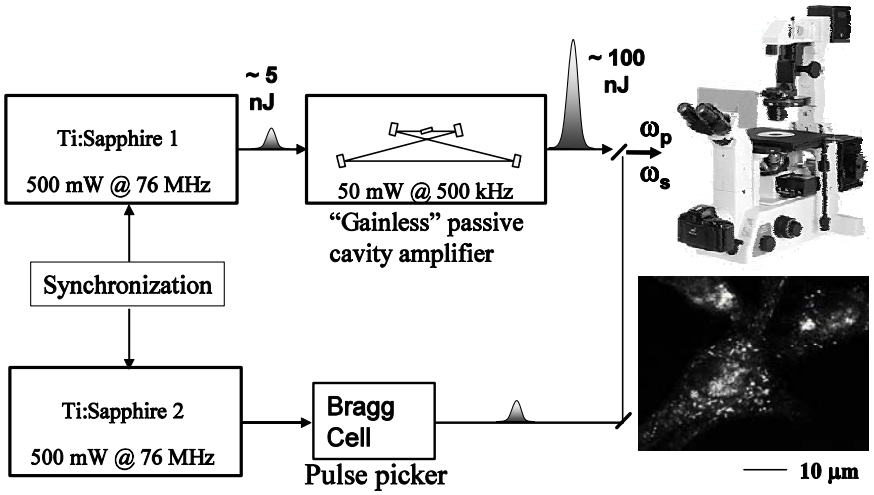

Figure 1-12. Schematic setup for coherent anti-Stokes Raman scattering (CARS) microscopy on living cells using two separate picosecond mode-locked lasers. The two lasers are tightly synchronized to minimize detection noise while the pump laser is enhanced in its peak power by a passive optical cavity. High *S/N* image of distribution of lipids in a live unstained fibroblast cell is achieved via resonant detection of C-H vibration frequency.

ACKNOWLEDGEMENTS

I would like to express my sincere appreciation and gratitude to my colleagues and collaborators, R.J. Jones, L. Chen, K. Holman, A. Marian, M. Stowe, D. Felinto, D.J. Jones, E. Potma, X.-S. Xie, S. Foreman, H. Kapteyn, S.T. Cundiff, T. Fortier, E. Ippen, and J. L. Hall. We gratefully acknowledge financial support from ONR, NASA, NIST, NSF, and the National Research Council for its Research Associate program.

REFERENCES

1. S. T. Cundiff and J. Ye, *Rev. Mod. Phys.* **75**, 325 (2003).
2. A. Baltuska, T. Udem, M. Uiberacker, M. Hentschel, E. Goulielmakis, C. Gohle, R. Holzwarth, V. S. Yakoviev, A. Scrinzi, T. W. Hansch and F. Krausz, *Nature* **421**, 611 (2003).
3. T. Udem, J. Reichert, R. Holzwarth and T. W. Hänsch, *Opt. Lett*. **24**, 881 (1999).
4. T. Udem, J. Reichert, R. Holzwarth and T. W. Hänsch, *Phys. Rev. Lett*. **82**, 3568 (1999).
5. J. Ye, T. H. Yoon, J. L. Hall, A. A. Madej, J. E. Bernard, K. J. Siemsen, L. Marmet, J.-M. Chartier and A. Chartier, *Phys. Rev. Lett.* **85**, 3797 (2000).
6. D. J. Jones, S. A. Diddams, J. K. Ranka, A. Stentz, R. S. Windeler, J. L. Hall and S. T. Cundiff, *Science* **288**, 635 (2000).
7. A. Apolonski, A. Poppe, G. Tempea, C. Spielmann, T. Udem, R. Holzwarth, T. W. Hänsch and F. Krausz, *Phys. Rev. Lett.* **85**, 740 (2000).
8. S. A. Diddams, T. Udem, J. C. Bergquist, E. A. Curtis, R. E. Drullinger, L. Hollberg, W. M. Itano, W. D. Lee, C. W. Oates, K. R. Vogel and D. J. Wineland, *Science* **293**, 825 (2001).
9. J. Ye, L. S. Ma and J. L. Hall, *Phys. Rev. Lett.* **87**, 270801 (2001).
10. J. D. Jost, J. L. Hall and J. Ye, *Optics Express* **10**, 515 (2002).
11. R. K. Shelton, L. S. Ma, H. C. Kapteyn, M. M. Murnane, J. L. Hall and J. Ye, *Science* **293**, 1286 (2001).
12. A. Baltuska, T. Fuji and T. Kobayashi, *Phys. Rev. Lett.* **88**, 133901 (2002).
13. L. Xu, C. Spielmann, A. Poppe, T. Brabec, F. Krausz and T. W. Hänsch, *Opt. Lett.* **21**, 2008 (1996).
14. H. R. Telle, G. Steinmeyer, A. E. Dunlop, J. Stenger, D. H. Sutter and U. Keller, *Appl. Phys.* B **69**, 327 (1999).
15. T. M. Fortier, D. J. Jones and S. T. Cundiff, *Opt. Lett.* **28**, 2198 (2003).
16. R. Ell, U. Morgner, F. X. Kärtner, J. G. Fujimoto, E. P. Ippen, V. Scheuer, G. Angelow, T. Tschudi, M. J. Lederer, A. Boiko and B. Luther-Davies, *Opt. Lett.* **26**, 373 (2001).
17. A. Bartels and H. Kurz, in *XIII International Conference on Ultrafast Phenomena*, edited by M. M. Murnane, N. F. Scherer, D. J. D. Miller and A. M. Weiner (OSA, Vancouver, BC, 2002), Vol. 72, p. 173.
18. J. K. Ranka, R. S. Windeler and A. J. Stentz, *Opt. Lett.* **25**, 25 (2000).
19. J. Reichert, R. Holzwarth, T. Udem and T. W. Hänsch, *Opt. Commun*. **172**, 59 (1999).
20. K. W. Holman, R. J. Jones, A. Marian, S. T. Cundiff and J. Ye, *Opt. Lett.* **28**, 851 (2003).
21. H. R. Telle, B. Lipphardt and J. Stenger, *Appl. Phys.* B **74**, 1 (2002).
22. S. A. Diddams, L. Hollberg, L. S. Ma and L. Robertsson, *Opt. Lett.* **27**, 58 (2002).
23. M. Niering, R. Holzwarth, J. Reichert, P. Pokasov, T. Udem, M. Weitz, T. W. Hänsch, P. Lemonde, G. Santarelli, M. Abgrall, P. Laurent, C. Salomon and A. Clairon, *Phys. Rev. Lett.* **84**, 5496 (2000).
24. J. Ye, J. L. Hall and S. A. Diddams, *Opt. Lett.* **25**, 1675 (2000).
25. G. Wilpers, T. Binnewies, C. Degenhardt, U. Sterr, J. Helmcke and F. Riehle, *Phys. Rev. Lett.* **89**, 230801 (2002).
26. R. J. Rafac, B. C. Young, J. A. Beall, W. M. Itano, D. J. Wineland and J. C. Bergquist, *Phys. Rev. Lett*. **85**, 2462 (2000).

27. L. Hollberg, C. W. Oates, E. A. Curtis, E. N. Ivanov, S. A. Diddams, T. Udem, H. G. Robinson, J. C. Bergquist, R. J. Rafac, W. M. Itano, R. E. Drullinger and D. J. Wineland, *IEEE J. Quantum Electron.* **37**, 1502 (2001).
28. J. Ye, L. Robertsson, S. Picard, L. S. Ma and J. L. Hall, IEEE Trans. *Instrum. Meas.* **48**, 544 (1999).
29. D. Felinto, C. A. C. Bosco, L. H. Acioli and S. S. Vianna, *Phys. Rev.* A **6406** (2001).
30. T. H. Yoon, A. Marian, J. L. Hall and J. Ye, *Phys. Rev.* A **63**, 011402 (2000).
31. J. E. Bjorkholm and P. F. Liao, *Phys. Rev. Lett.* **33**, 128 (1974).
32. O. Poulsen and N. I. Winstrup, *Phys. Rev. Lett.* **47**, 1522 (1981).
33. R. Teets, J. Eckstein and T. W. Hänsch, *Phys. Rev. Lett.* **38**, 760 (1977).
34. M. J. Snadden, A. S. Bell, E. Riis and A. I. Ferguson, *Opt. Commun.* **125**, 70 (1996).
35. A. Marian, X. Xu and J. Ye, Bulletin *Am. Phys. Soc.* **48**, 136 (2003).
36. T. M. Fortier, D. J. Jones, J. Ye, S. T. Cundiff and R. S. Windeler, *Opt. Lett.* **27**, 1436 (2002).
37. R. K. Shelton, S. M. Foreman, L. S. Ma, J. L. Hall, H. C. Kapteyn, M. M. Murnane, M. Notcutt and J. Ye, *Opt. Lett.* **27**, 312 (2002).
38. S. M. Foreman, D. J. Jones and J. Ye, *Opt. Lett.* **28**, 370 (2003).
39. R. J. Jones and J. Ye, *Opt. Lett.* **27**, 1848 (2002).
40. E. O. Potma, D. J. Jones, J. X. Cheng, X. S. Xie and J. Ye, *Opt. Lett.* **27**, 1168 (2002).
41. E. O. Potma, C. Evans, X. S. Xie, R. J. Jones and J. Ye, *Opt. Lett.* **28**, 1835 (2003).
42. L. S. Chen and J. Ye, *Chem. Phys. Lett.* **381**, 777 (2003).
43 W. Y. Cheng, L. S. Chen, T. H. Yoon, J. L. Hall and J. Ye, *Opt. Lett.* **27**, 571 (2002).
44. J. Vigué, M. Broyer and J. C. Lehmann, *Phys. Rev. Lett.* **42**, 883 (1979).
45. C. J. Bordé, G. Camy, B. Decomps and J.-P. Descoubes, *J. Physique* **42**, 1393 (1981).
46. J. P. Pique, F. Hartmann, S. Churassy and R. Bacis, *J. Physique* **47**, 1917 (1986).
47. B. Bodermann, H. Knockel and E. Tiemann, *Eur. Phys. J.* D **19**, 31 (2002).
48. R. J. Jones, W. Y. Cheng, K. W. Holman, L.-S. Chen, J. L. Hall and J. Ye, *Appl. Phys.* B **74**, 597 (2002).
49. K. W. Holman, D. J. Jones, J. Ye and E. P. Ippen, *Opt. Lett.* **28**, 2405 (2003).
50. R. J. Jones and J. C. Diels, *Phys. Rev. Lett.* **86**, 3288 (2001).
51. A. Volkmer, J. X. Cheng and X. S. Xie, *Phys. Rev. Lett.* **8702** (2001).
52. L. D. Book, J. X. Cheng, A. Volkmer and X. S. Xie, *Biophysical Journal* **80**, 171A (2001).